Electronic Supplementary Material (ESI) for Journal of Materials Chemistry A.

Electronic Supplementary Information

Ferroconcrete-inspired design of nonwoven graphene fiber fabrics enforced electrode toward flexible fast-charging sodium ion storage device

Zexin Liu[a, b†], Xin Zhang[a, b†], Cai Liu[a, b], Dongyang Li[a, b], Miaoxin Zhang, Fuxing Yin [a, b], Guoqing Xin[c*], Gongkai Wang[a, b*]

[a] *School of Material Science and Engineering, Research Institute for Energy Equipment Materials, Hebei University of Technology, Tianjin, 300130, China*

[b] *Tianjin Key Laboratory of Materials Laminating Fabrication and Interface Control Technology, Hebei University of Technology, Tianjin 300130, China*

[c] *Wuhan National High Magnetic Field Center，Huazhong University of Science and Technology, Wuhan 430074, China*

**Corresponding authors.*

E-mail addresses:

wang.gongkai@hebut.edu.cn (G. K. Wang), guoqingxin@hust.edu.cn (G. Q. Xin)

[†]*Z.X.L and X.Z. contributed equally to this work.*

Calculation

The specific calculations are followed the equations as below:

Energy density (E, W h kg^{-1} or Wh cm^{-3}) $$E = \int Q dV = \int_{t_1}^{t_2} IV_{(t)}\, dt = \frac{\int_{t_1}^{t_2} IV_{(t)}\, dt}{A} \quad (1)$$

Power density (P, W kg^{-1} or W cm^{-3}) $$P = \frac{E}{t} \quad (2)$$

where t_1 is the initial time of discharge, and t_2 is the moment that the discharge ends, *I* is the constant current applied to the device, $V_{(t)}$ is the discharge voltage at t, d*t* is time differential, and A is the total mass of the entire anode and cathode or the volume of the entire device (including the anode, cathode, separator, and plastic package). The energy density should be calculated through the integration of the galvanostatic charge/discharge curve.

Table S1 Parameters of calculated conductivity.

Sample	L (m)	W (m)	H (m)	R (Ω)	Conductivity (S m^{-1})
GF	0.0098	0.00052	0.000166	14.8	7671
Bi/GF	0.0086	0.00052	0.000184	6.67	13475

Table S2 Relevant parameters of the compared devices in Ragone plots.

	Anode thickness (μm)/ loading(mg cm^{-2})	Separators (μm)	Cathode thickness (μm)/ loading(mg cm^{-2})	Device thickness (μm)
This work	256 / 9.8	52	783 / 34.2	1175
Co_9S_8 // Co_3O_4@RuO_2	-/ -	-	-/ -	1000
NiO(carbon cloth)//ZnO	-/-	-	-/-	800
$Li_4Ti_5O_{12}$ (carbon cloth)//CNT	-/ 4	-	-/ 2.34	691
$Na_2Ti_3O_7$/CT (carbon textiles) rGO	-/-	-	-/-	1500
$Ni_{0.25}Mn_{0.75}O$ (Ti foil) //AC	-/-	-	-/-	170.57
Nb_2O_5 // AC	-/-	-	-/-	100
Li-thin film battery	-/-	-	-/-	-
TiO_2@MnO_2//TiO_2 @C-ASCS	-/-	-	-/-	-
CoO@PPY // AC	-/ 1.98	-	-/ 8	-
PANI//WO_x@MoO_x-ASCs	-/-	40	-/-	-

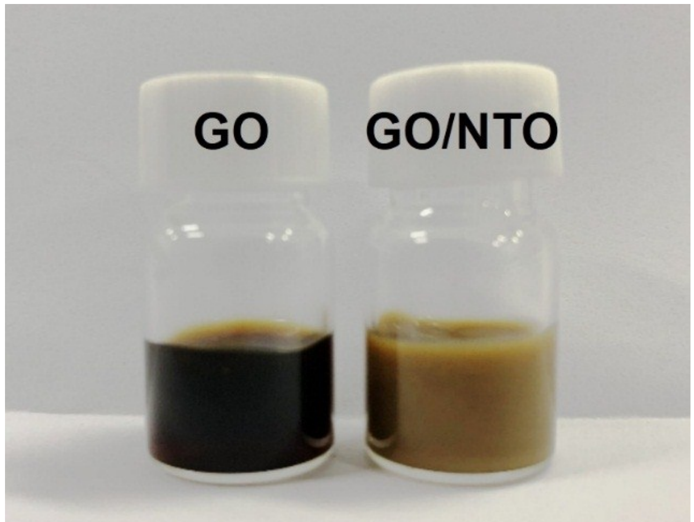

Fig. S1 Digital image of GO/DMF and GO/NTO/DMF solution.

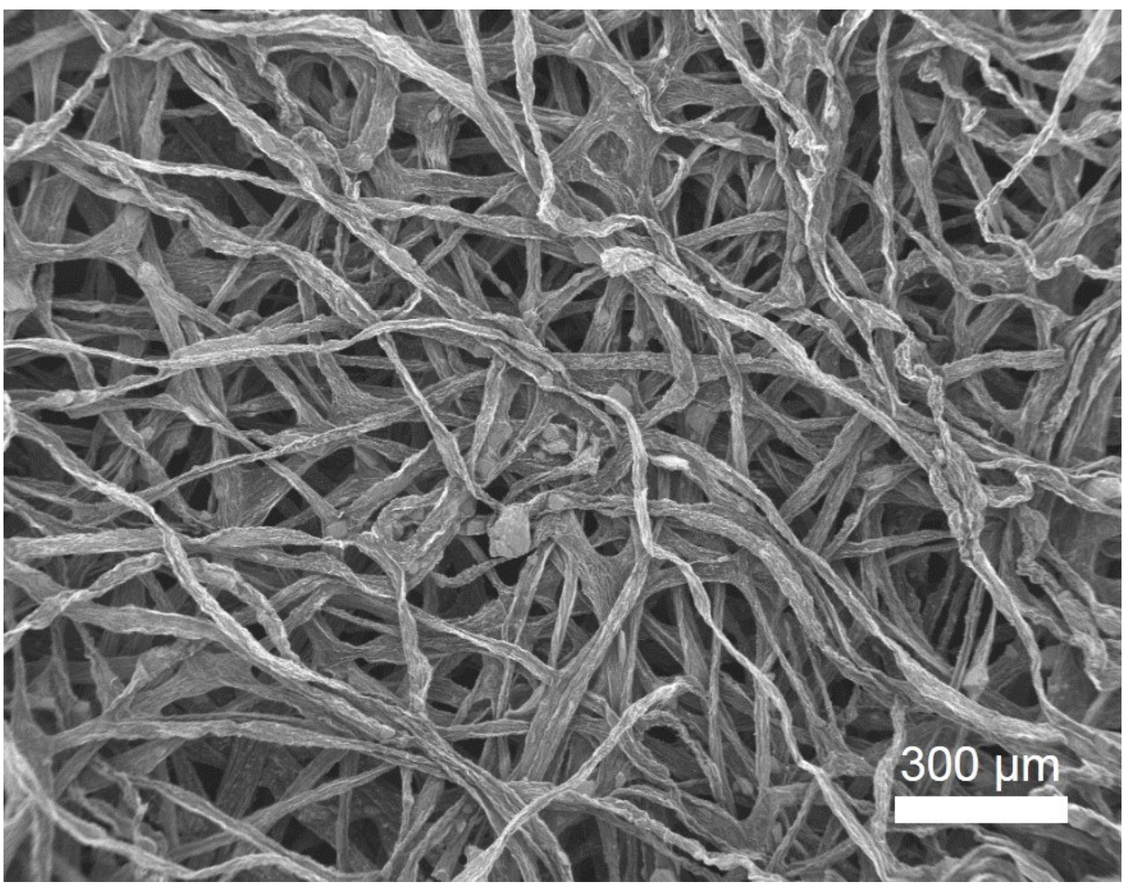

Fig. S2 Top view of Bi/GF nonwoven fabric

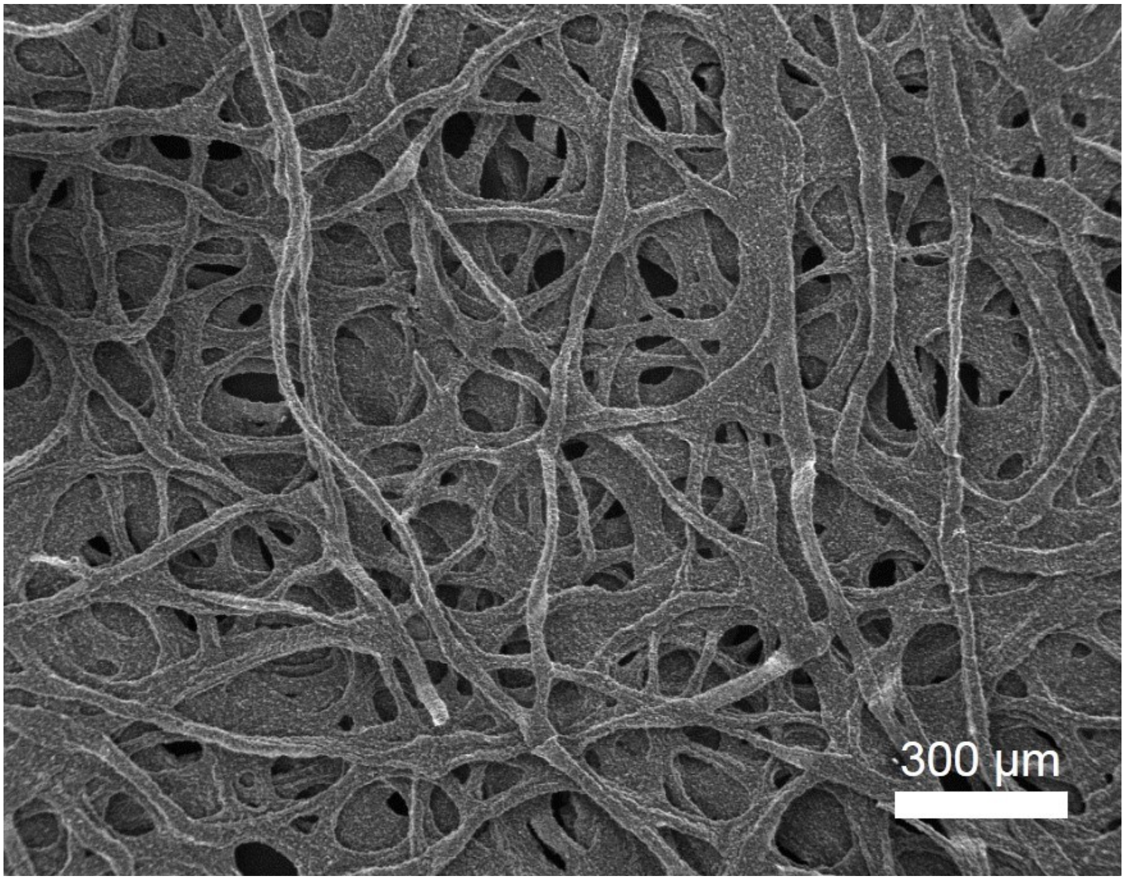

Fig. S3 Top view of AC/GF nonwoven fabric

Characterizations of various active materials

For the 1D NTO nanorods/GF nonwoven fabrics (Fig. 2(c)-(d)), the phase structure of $Na_2Ti_7O_{15}$ (Space group: C2/m, JCPDS No. 76-1648) is confirmed by the X-ray diffraction (XRD) pattern (Fig. S4), consistent with our previous report.[1] The X-ray photoelectron spectroscopy (XPS) spectrum of C 1s demonstrates the well-reduced GO sheets (Fig. S5). About 70 wt.% NTO is contained in the fabrics (Fig. S6), and due to the 1D nanorod geometry (characterized by the scanning electron microscope (SEM) and transmission electron microscopy (TEM), Fig. S7), NTOs hybridize with graphene sheets densely and are strongly confined in the graphene fiber, in favor of electron transport with each other. For the 2D $MoSe_2$/graphene fiber nonwoven fabrics, the phase structure of $MoSe_2$ is well-indexed to the JCPDS No. 29-0914 (Fig. S8). The morphology of the $MoSe_2$ nano-flower coating on graphene nanosheets is characterized (Fig. S9), and the weight percentage of bare $MoSe_2$ is about 70 wt.% (Fig. S10). In the case of the 3D active materials, bulk Bi (The XRD pattern that corresponds to the JCPDS No. 85-1329 is shown in Fig. S12) and AC powders (Kuraray Chemical Co., Ltd., YP-50F) were incorporated in the fabrics. Due to the different densities of Bi and AC, the volumetric distribution in the fabrics is different at the same mass ratio of 70 wt.% (Fig. S13). The Bi powder with the size of ~70 μm (Fig. S14) and the AC with the size of ~5 μm can be well-wrapped in the fibers, maintaining the conductive connection and flexibility of the fabrics benefited from the raw large-sized GO sheets.

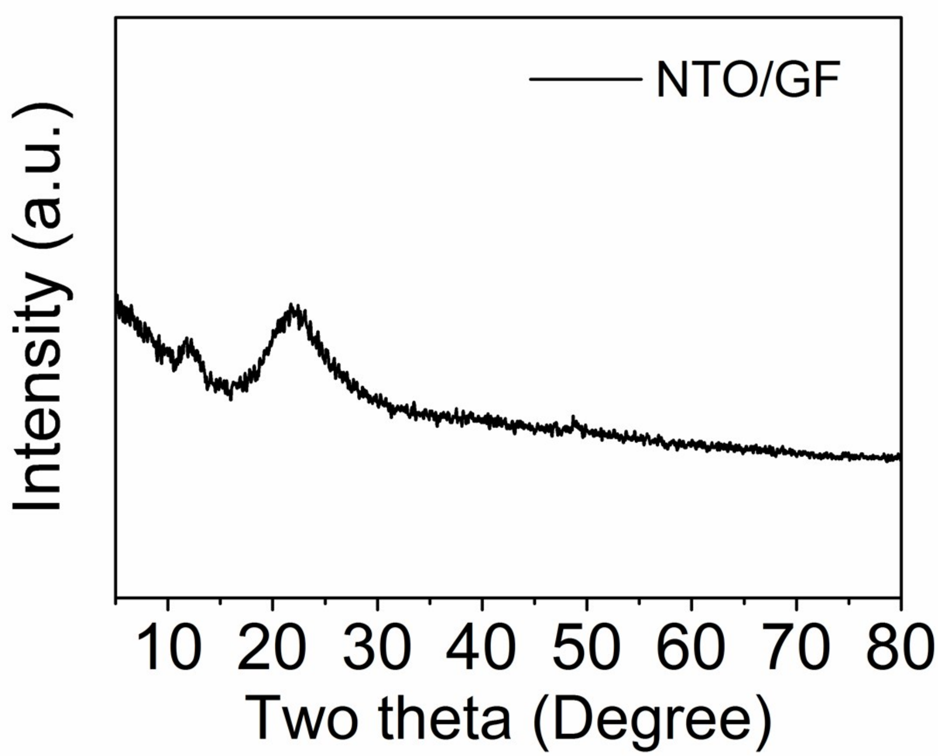

Fig. S4 XRD pattern of NTO/GF nonwoven fabric.

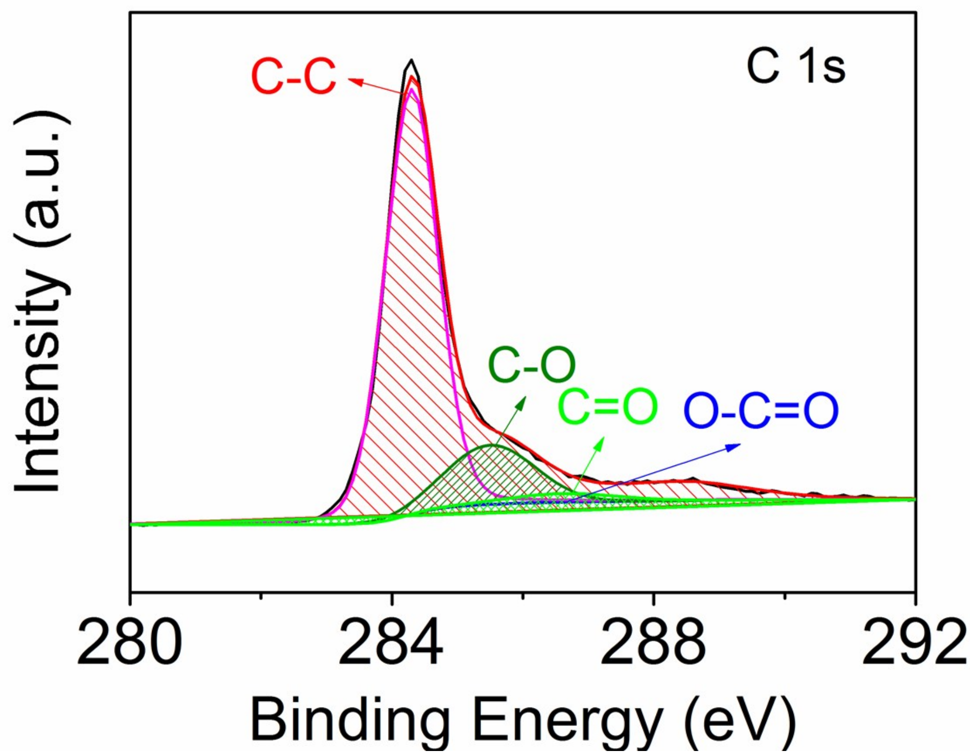

Fig. S5 XPS spectrum of C 1s of NTO/GF nonwoven fabric.

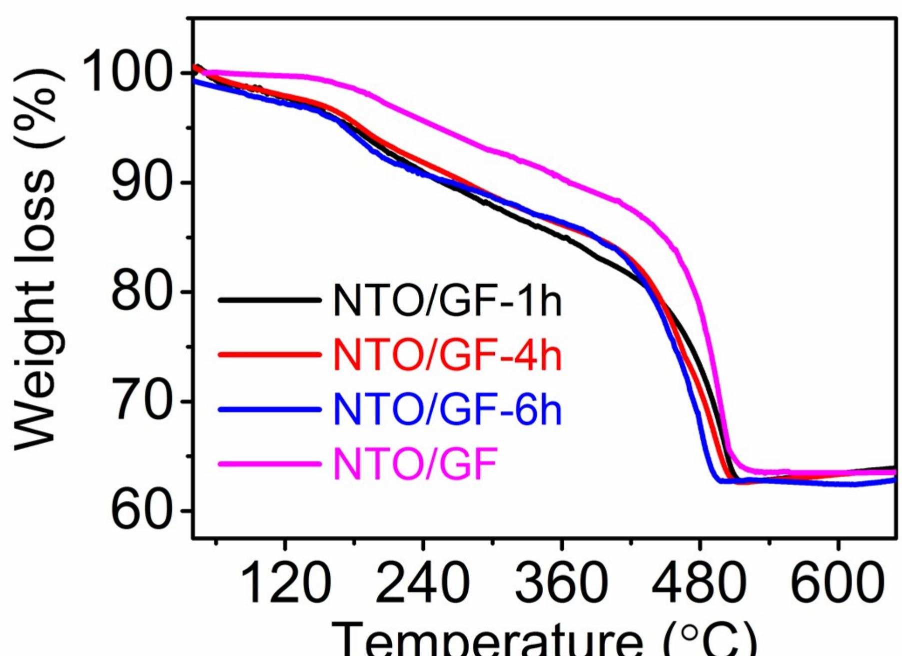

Fig. S6 TGA curves of NTO/GF nonwoven fabrics with various etching durations.

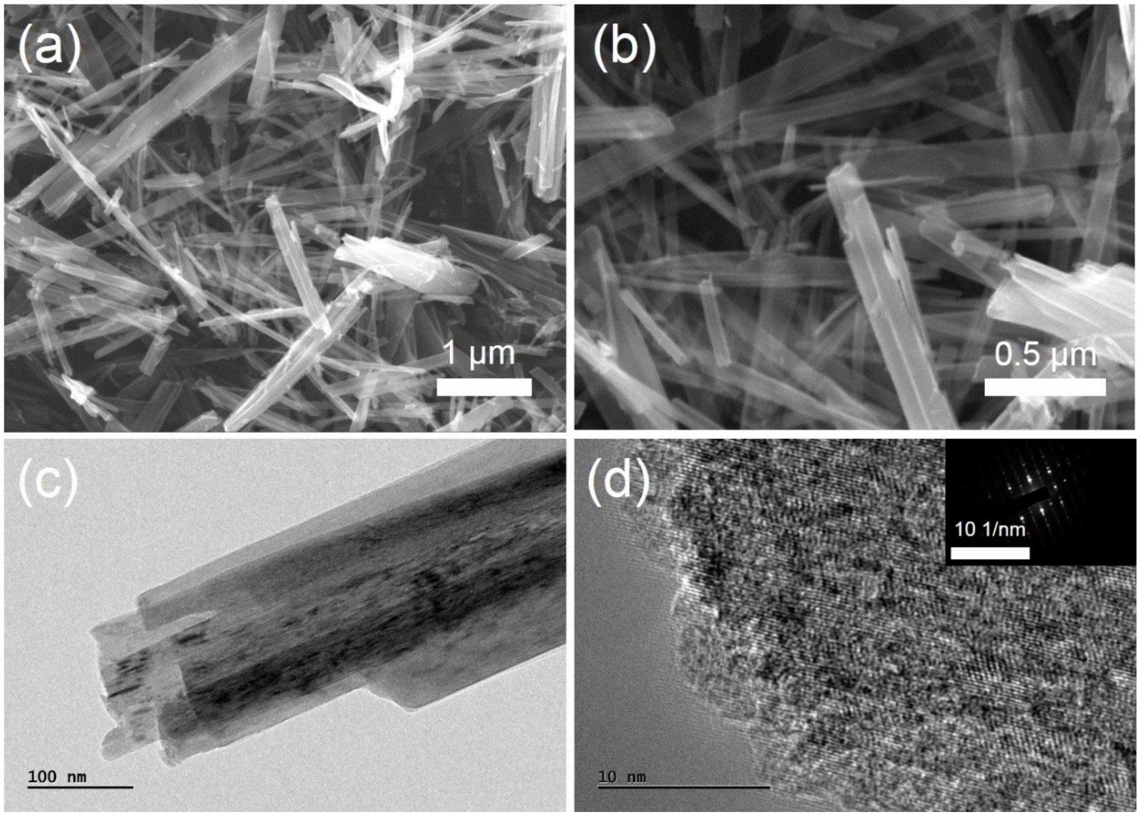

Fig. S7 Morphology of bare NTO nanorods: (a, b) SEM images. (c, d) TEM images.

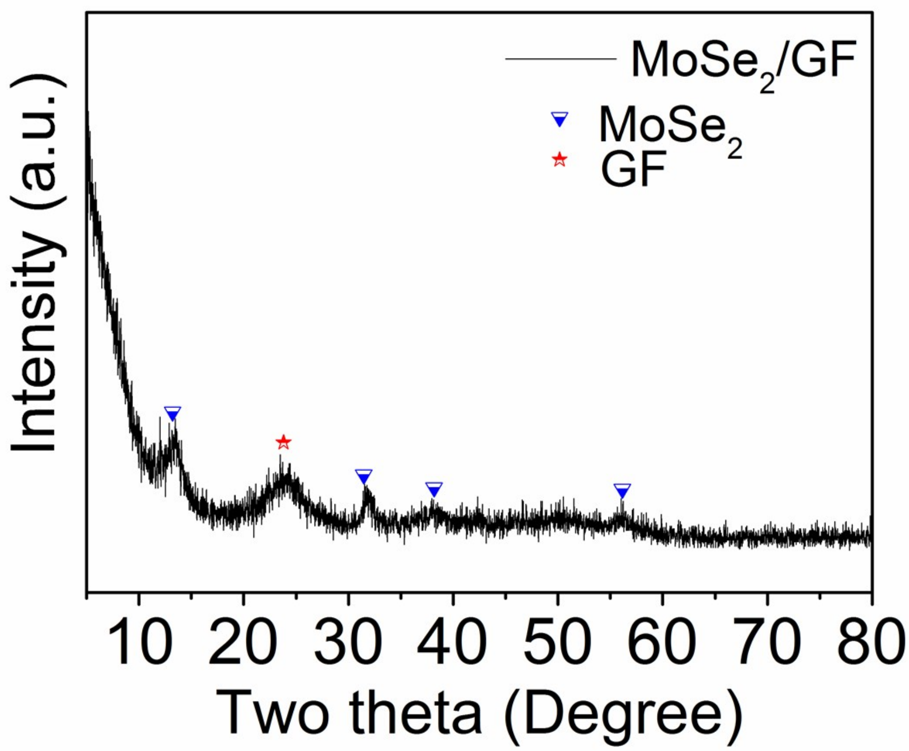

Fig. S8 XRD pattern of $MoSe_2$/GF nonwoven fabric.

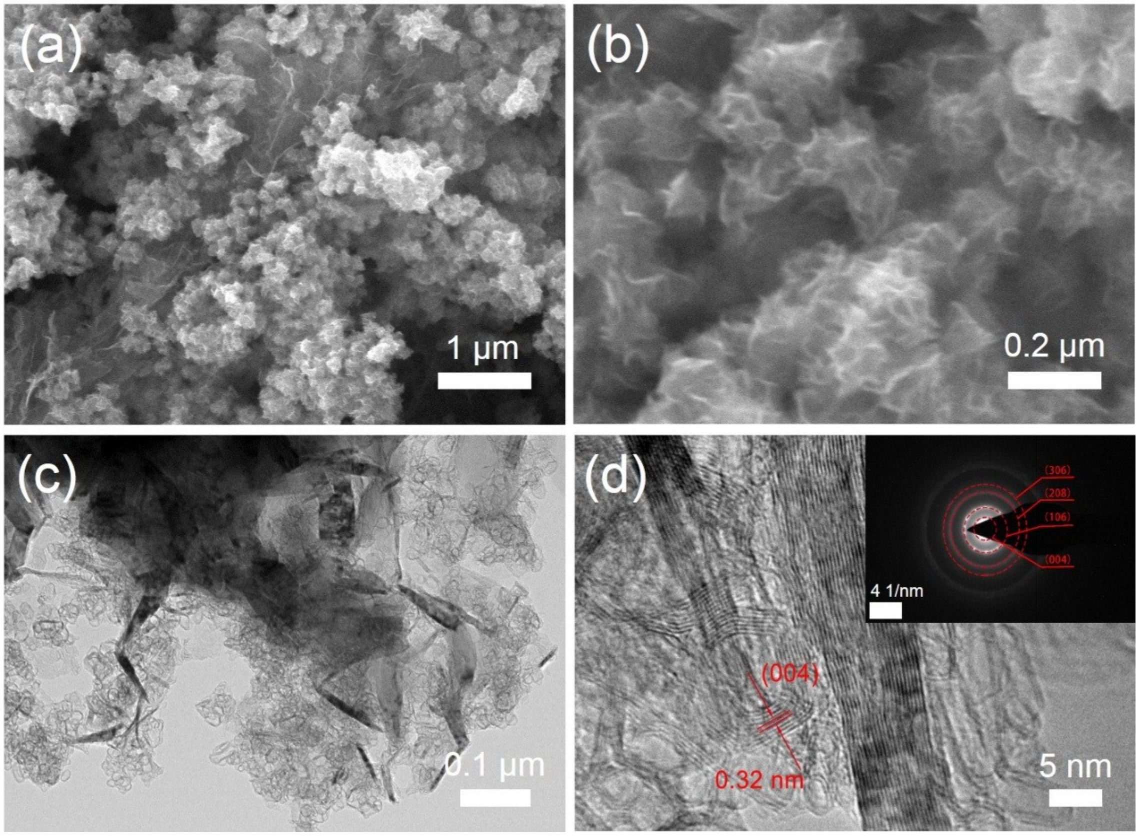

Fig. S9 Morphology of $MoSe_2$/graphene nanosheets: (a, b) SEM images. (c, d) TEM images.

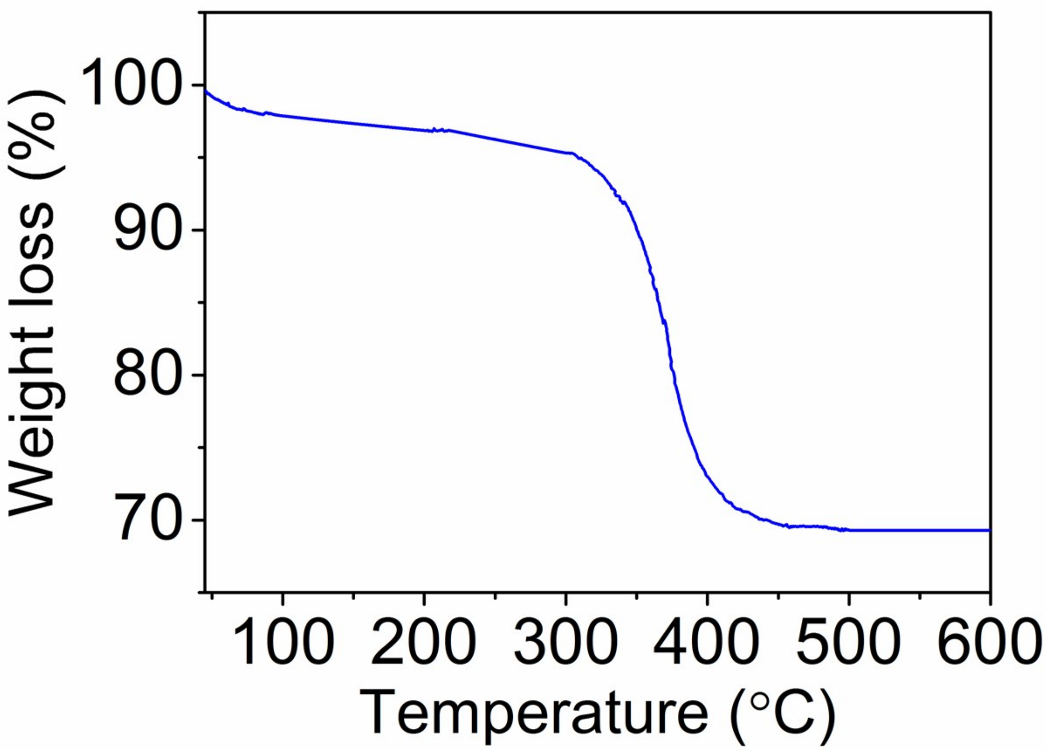

Fig. S10 TGA curve of $MoSe_2$/GF nonwoven fabric.

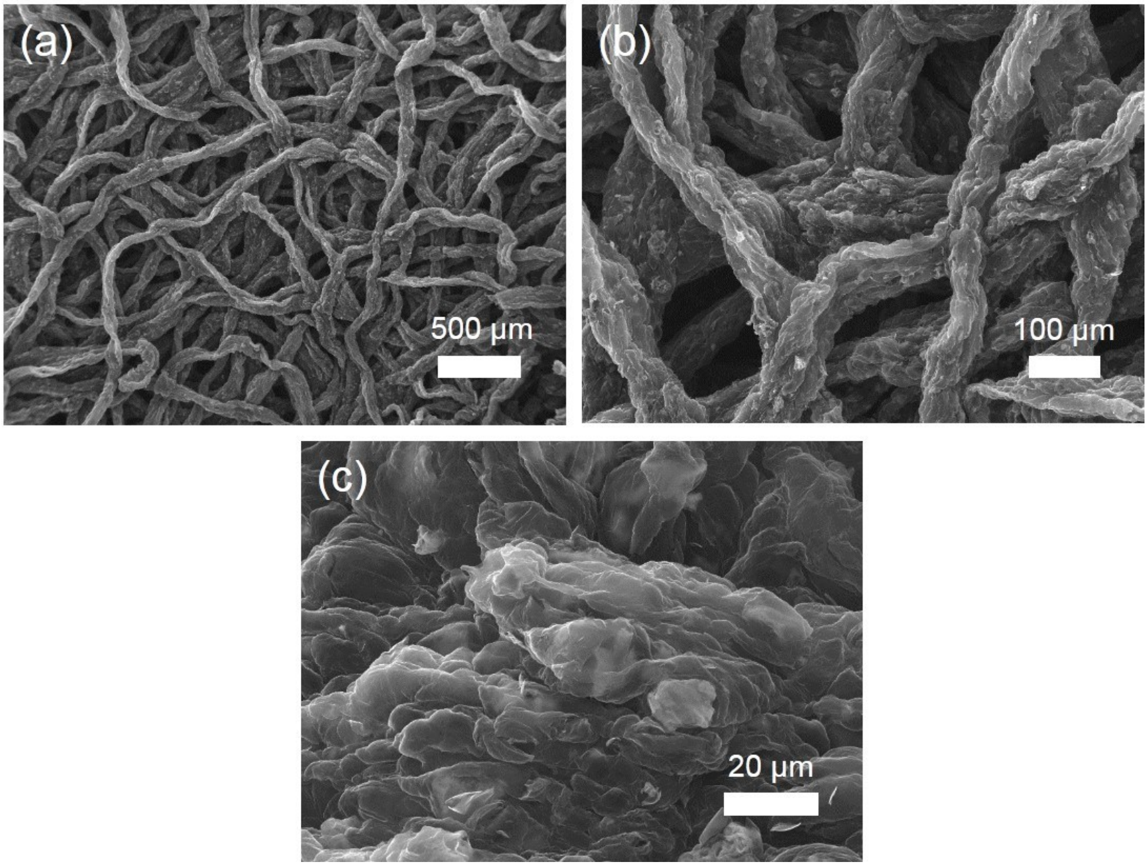

Fig. S11 Top view of SEM images of $MoSe_2$/GF nonwoven fabric.

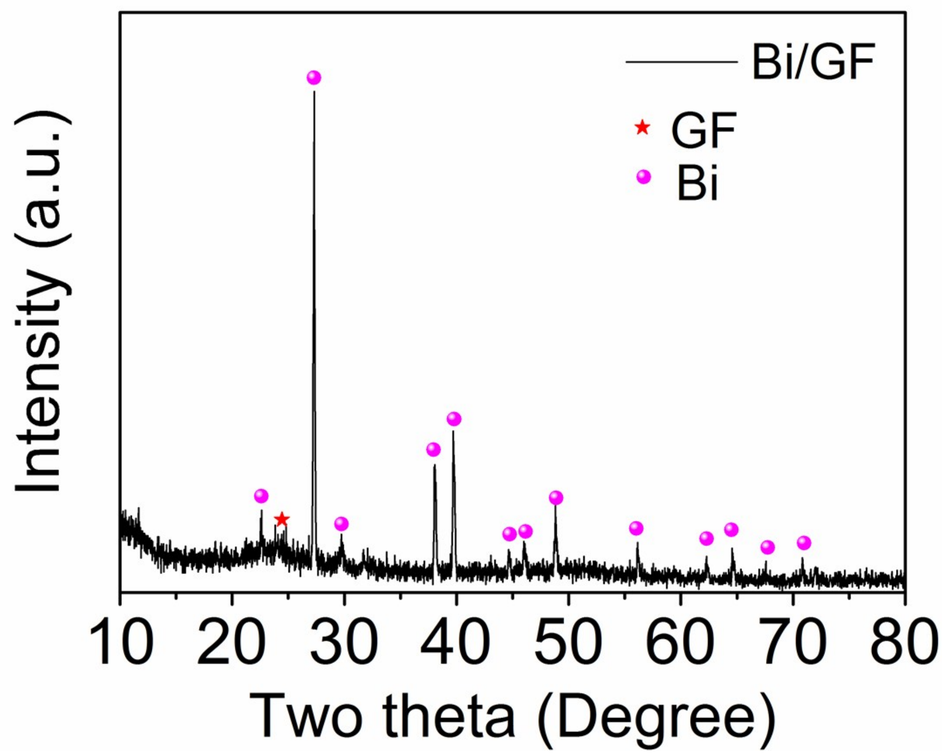

Fig. S12 XRD pattern of Bi/GF nonwoven fabric

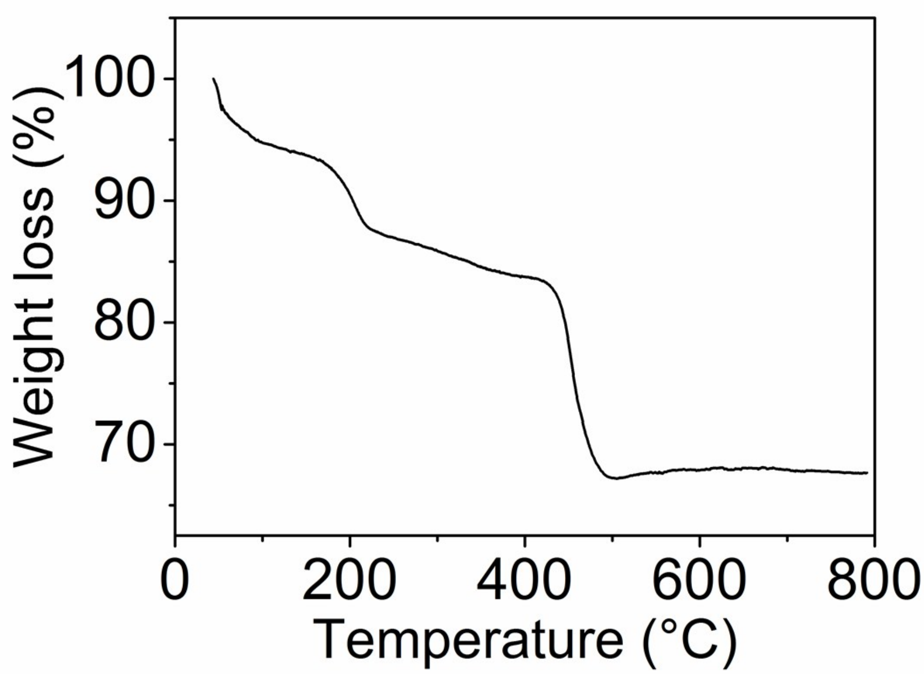

Fig. S13 TGA curve of Bi/GF nonwoven fabric.

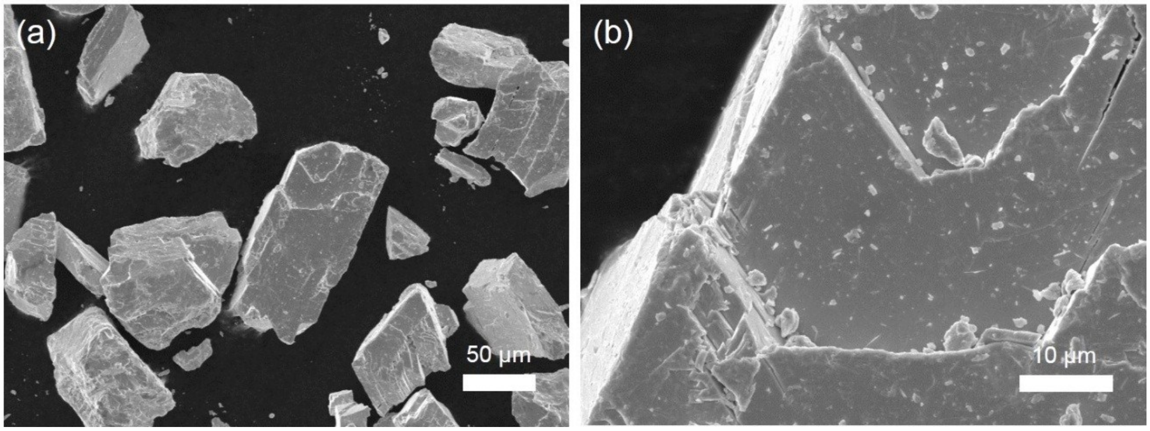

Fig. S14 SEM images of bare Bi powder.

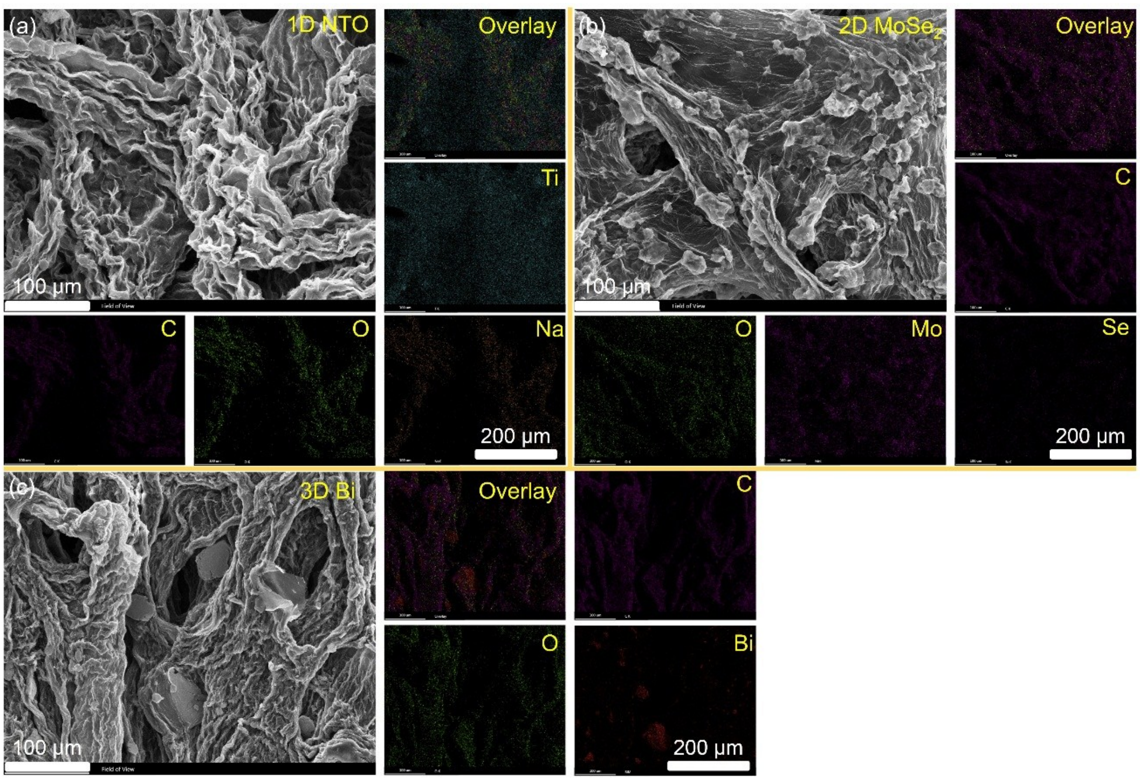

Fig. S15 EDS mapping of NTO/GF, $MoSe_2$/GF, and Bi/GF nonwoven fabrics.

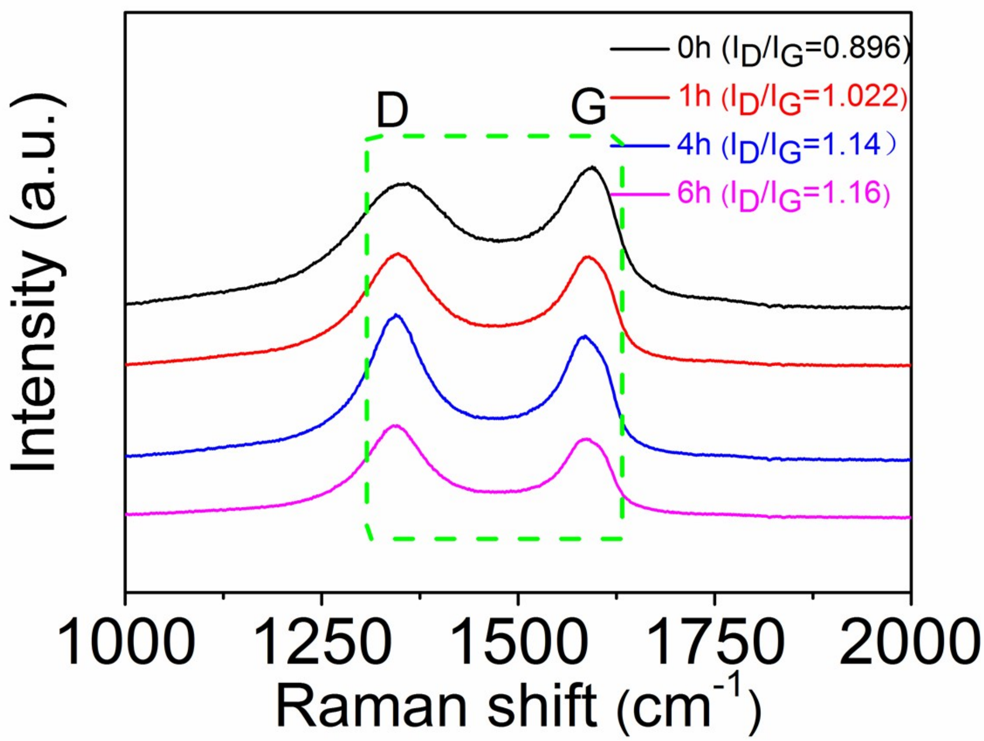

Fig. S16 Raman spectra of GO with various etching duration.

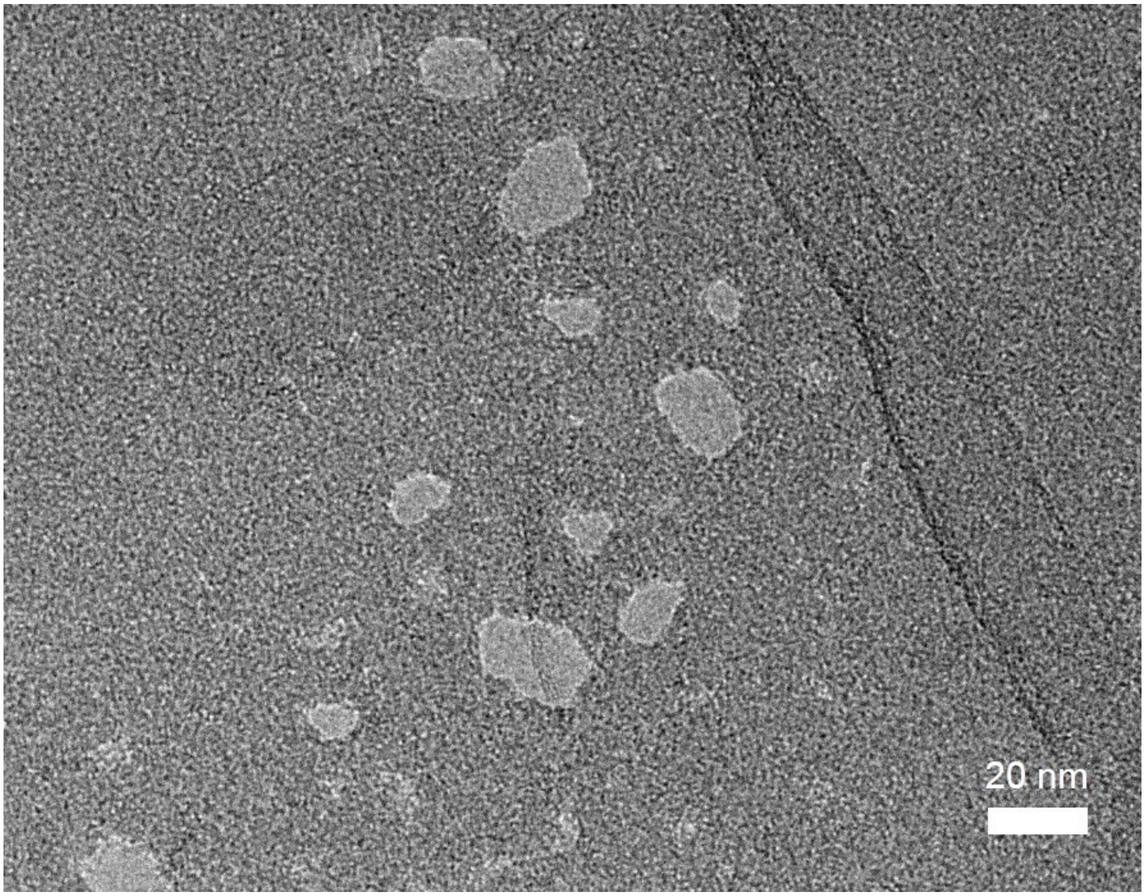

Fig. S17 TEM image of GO etched 4 h.

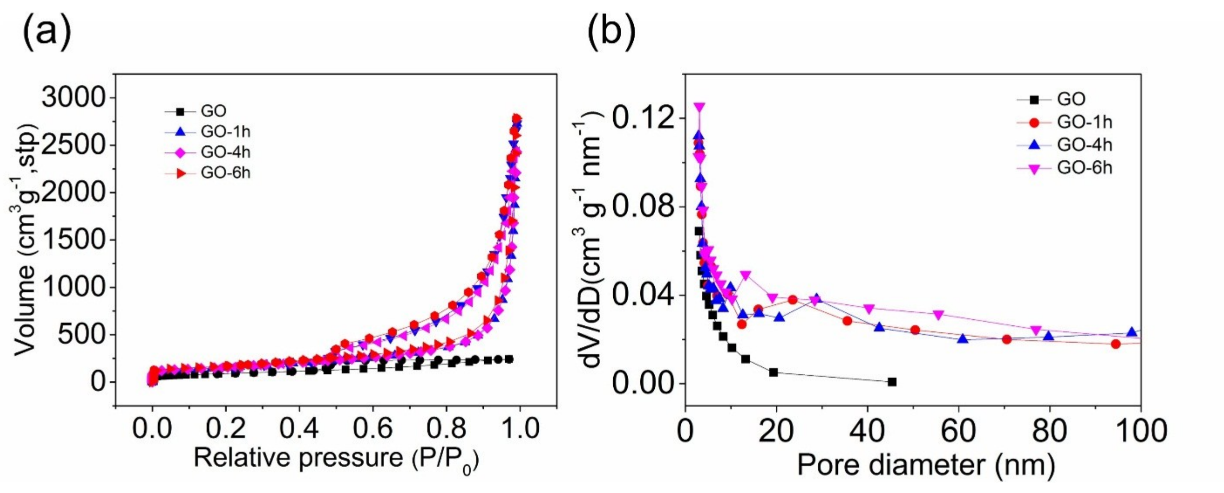

Fig. S18 (a) N_2 sorption/desorption isotherms and (b) corresponding BJH pore size distribution of GO and pore-etched GO.

The specific surface areas of GO, GO-1h, GO-4h, and GO-6h are 320, 532, 550 and 595 $m^2 g^{-1}$, respectively. The corresponding BJH pore size distribution is dramatically different between GO and pore-etched GO. The pore-etched GO showed a created pore size distribution up to the range of ~100 nm, demonstrating the occurrence of etching reaction. By extending the reaction time, the pore density in the GO plane increased.

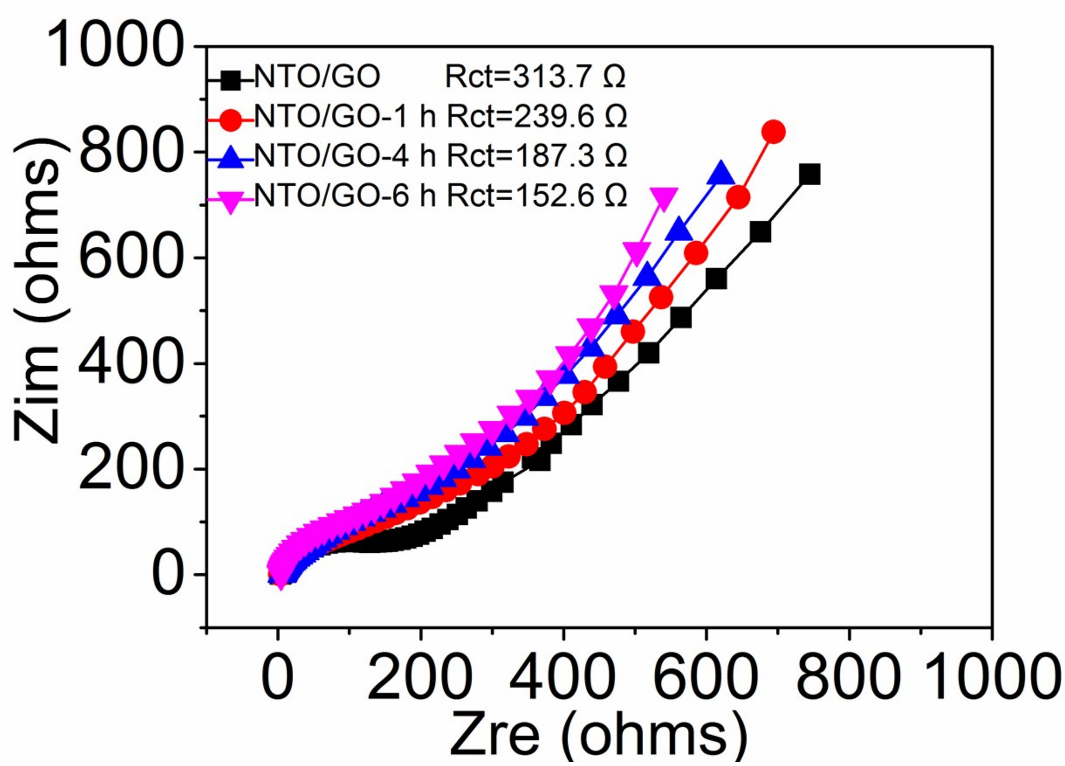

Fig. S19 EIS spectra of NTO/GO and NTO/pore-etched GO.

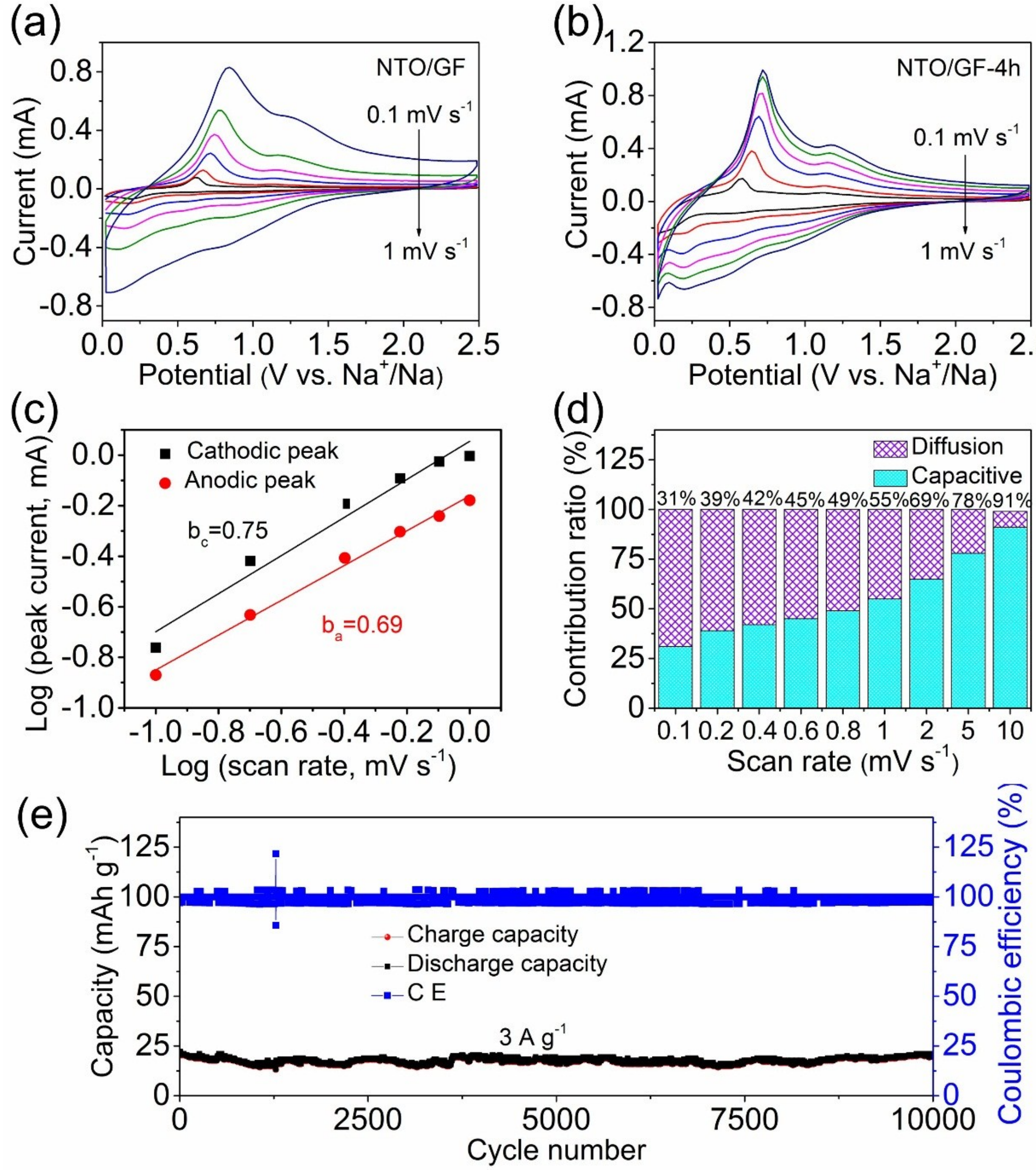

Fig. S20 (a, b) CV curves of NTO/GF and NTO/GF-4h nonwoven fabrics. NTO/GF-4h nonwoven fabrics: (c) Logarithm of peak current as a function of scan rate. (d) Contribution ratio of capacity at various scan rates. (e) Cyclic behavior at the current density of 3 A g^{-1}.

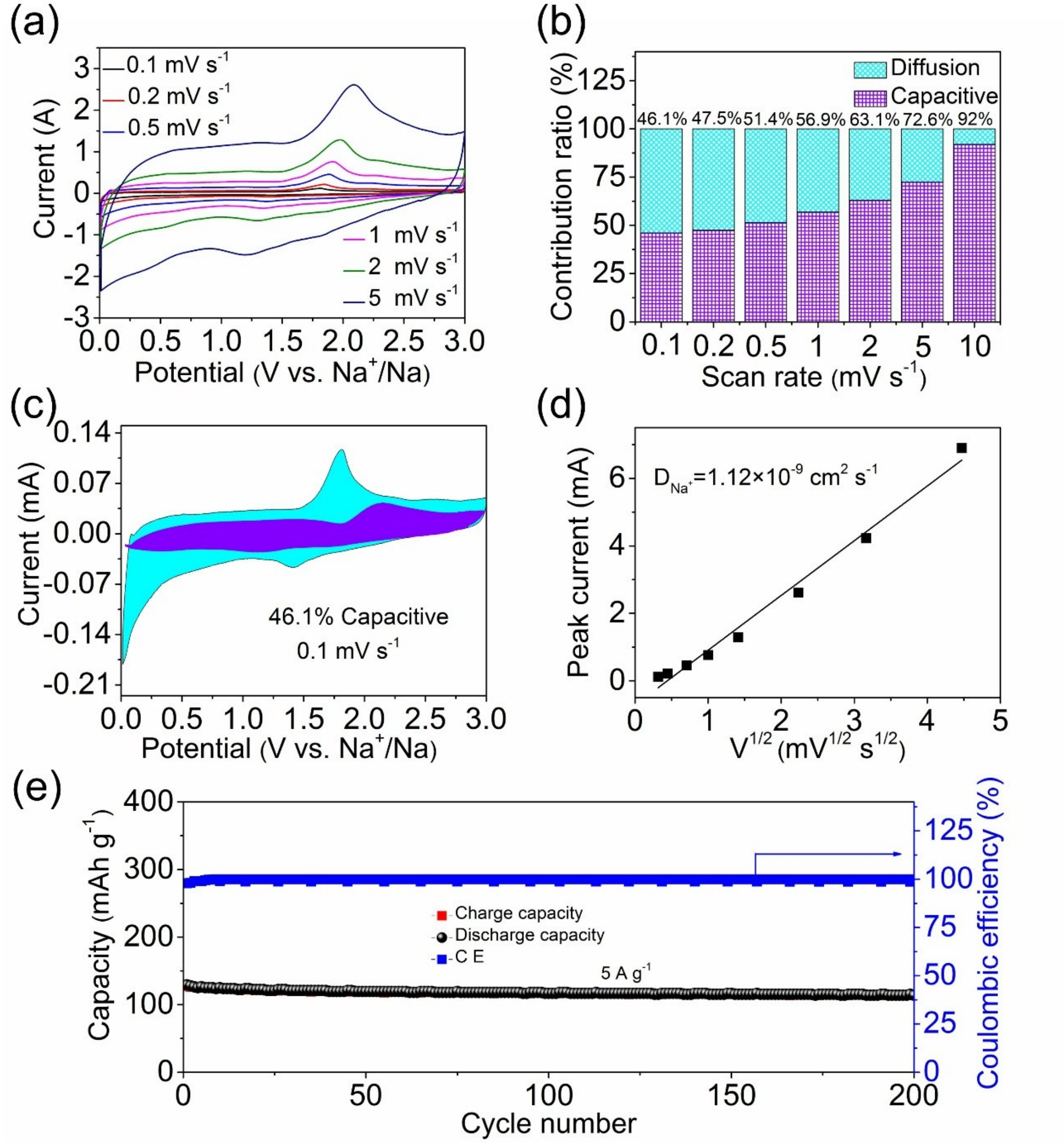

Fig. S21 Electrochemical performances of $MoSe_2$/GF-4h nonwoven fabric: (a) CV curves at various scan rates. (b) Contribution ratio of capacity at various scan rates. (c) CV curve at the scan rate of 0.4 mV s^{-1}, and corresponding capacitive contribution region (purple). (d) Dependence of peak current on the square root of the scan rate. (e) Cyclic behavior at the current density of 5 A g^{-1}.

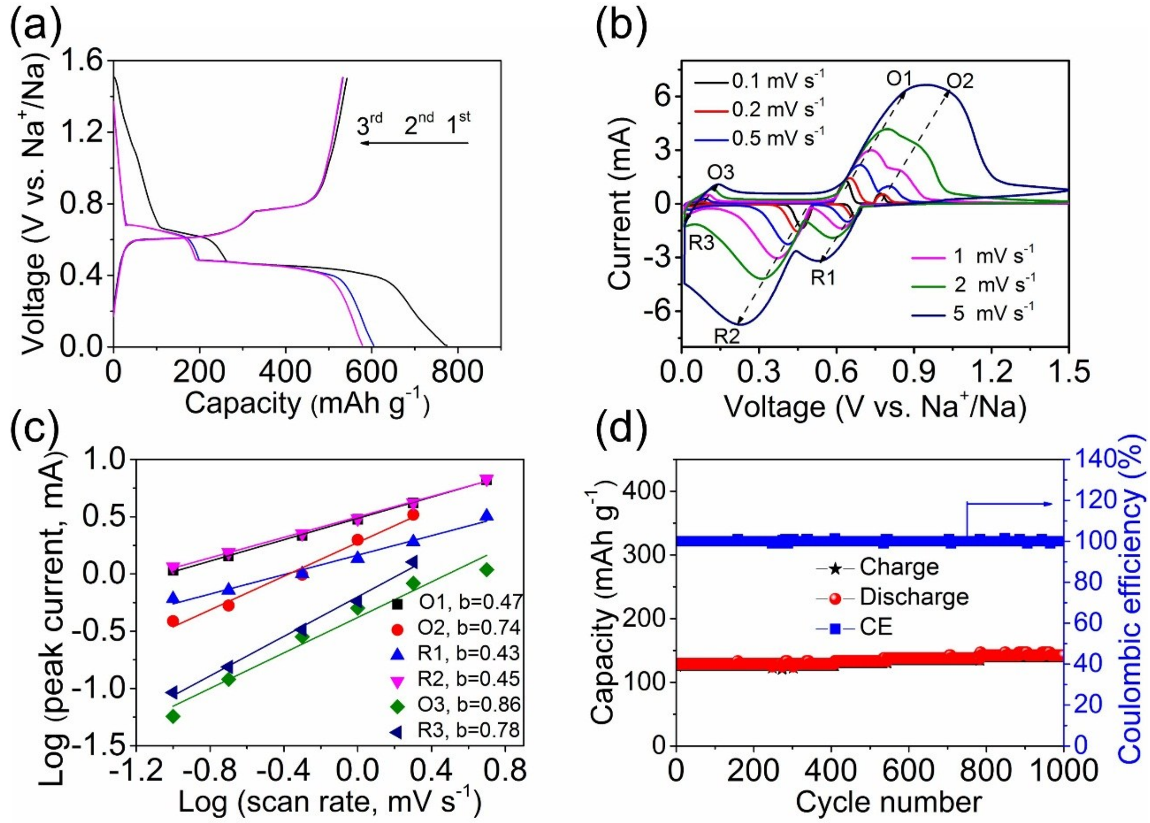

Fig. S22 Electrochemical performances of Bi/GF-4h nonwoven fabric: (a) Initial three galvanostatic charge/discharge curves. (b) CV curves at various scan rates. (c) Logarithm of peak current as a function of scan rate. (d) Cyclic life at the ultra-high current density of 44.8 A g^{-1}.

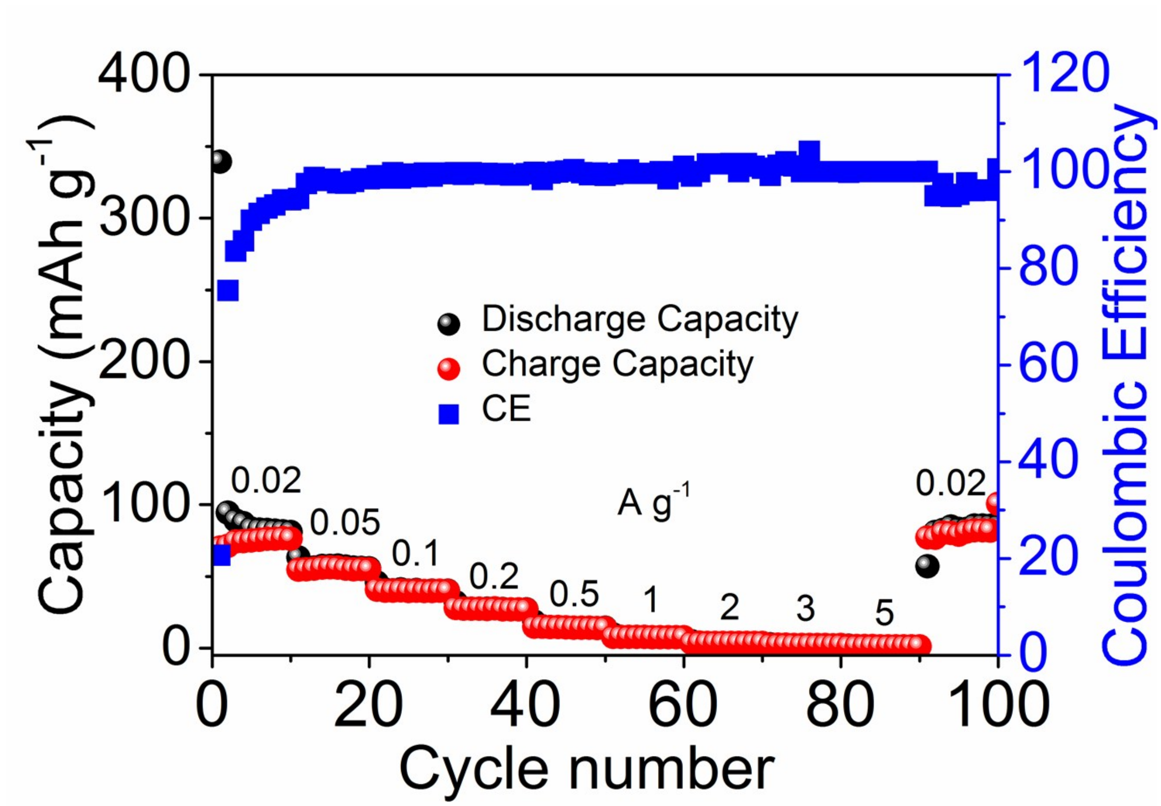

Fig. S23 Specific capacity of bare GF at various current densities.

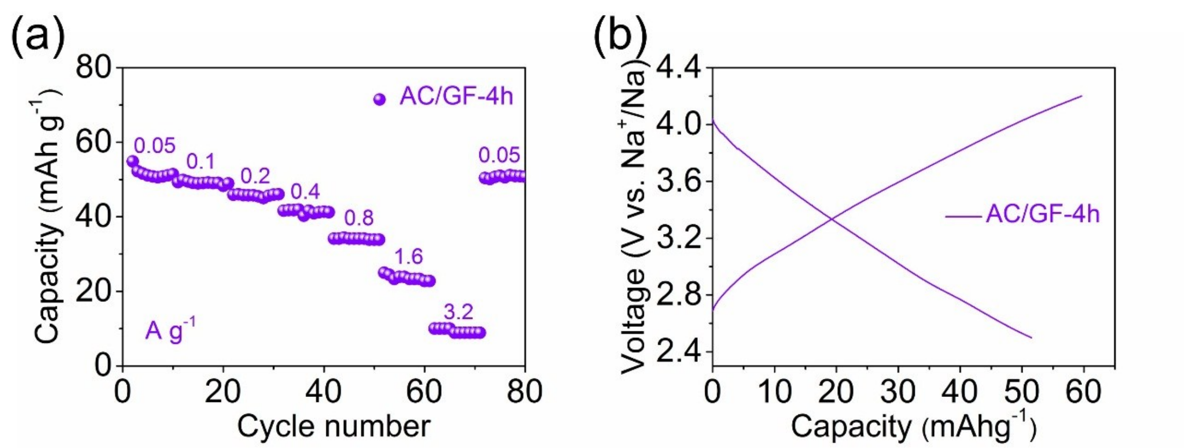

Fig. S24 Electrochemical performances of AC/GF-4h nonwoven fabric: (a) Rate performance at different current densities. (b) Typical galvanostatic charge/discharge curve.

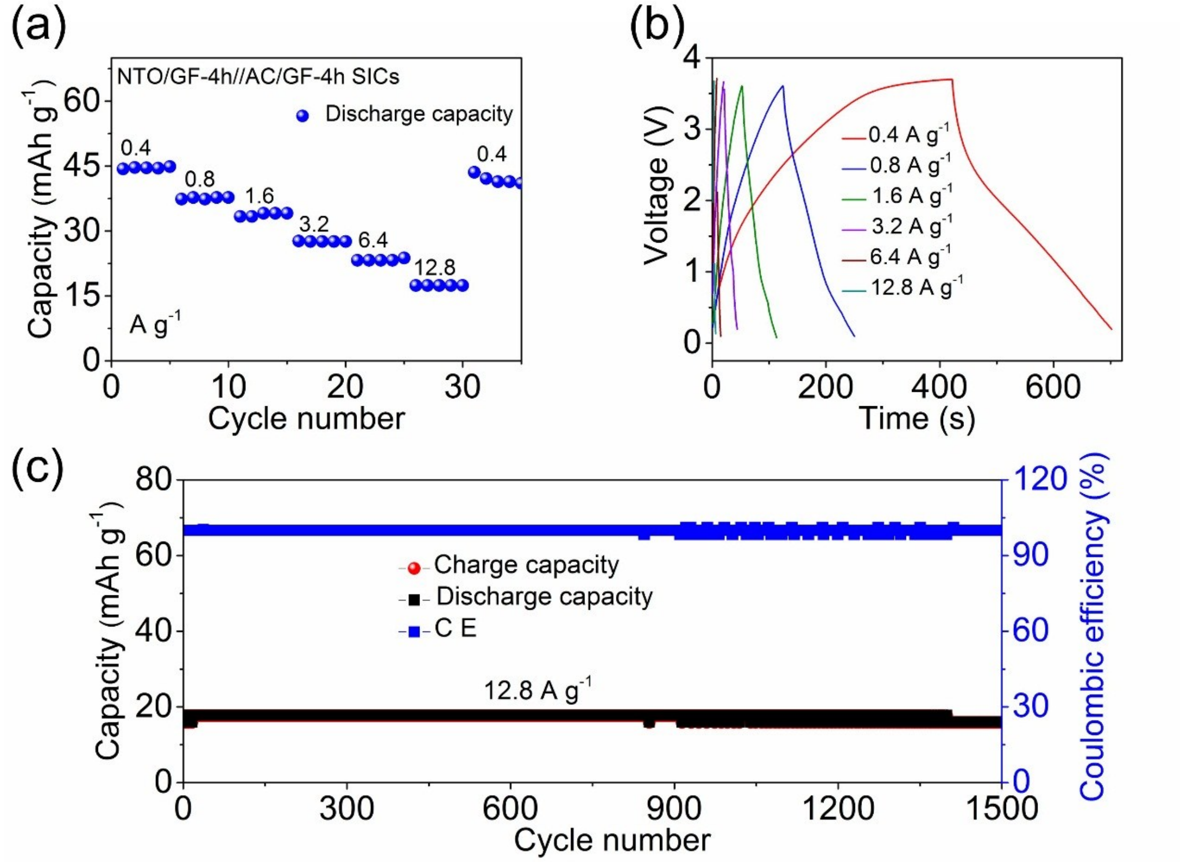

Fig. S25 Electrochemical performances of SICs based on NTO/GF-4h and AC/GF-4h fabrics electrodes: (a) Rate performance. (b) Galvanostatic charge/discharge curves at various current densities. (c) Cyclic life at the current density of 12.8 A g^{-1}.

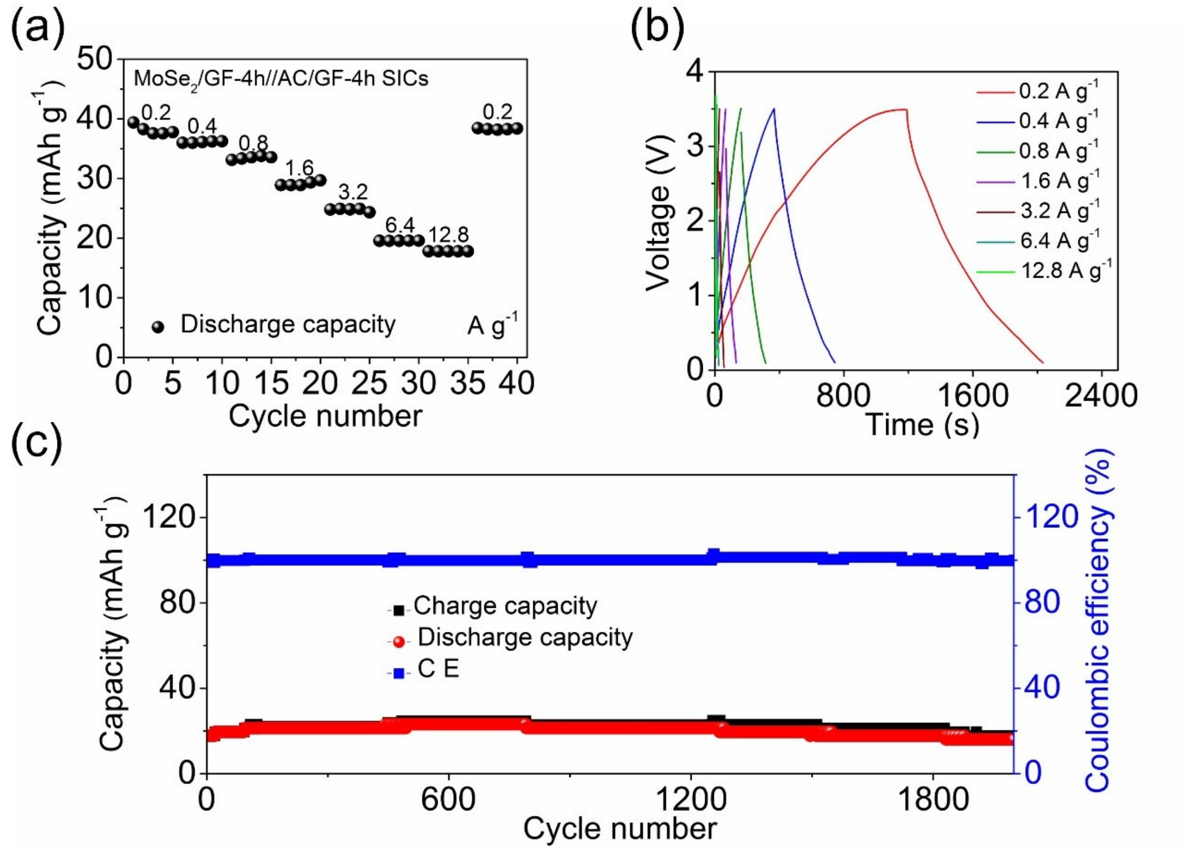

Fig. S26 Electrochemical performances of SICs based on $MoSe_2$/GF-4h and AC/GF-4h fabrics electrodes: (a) Rate performance. (b) Galvanostatic charge/discharge curves at various current densities. (c) Cyclic life at the current density of 12.8 A g^{-1}.

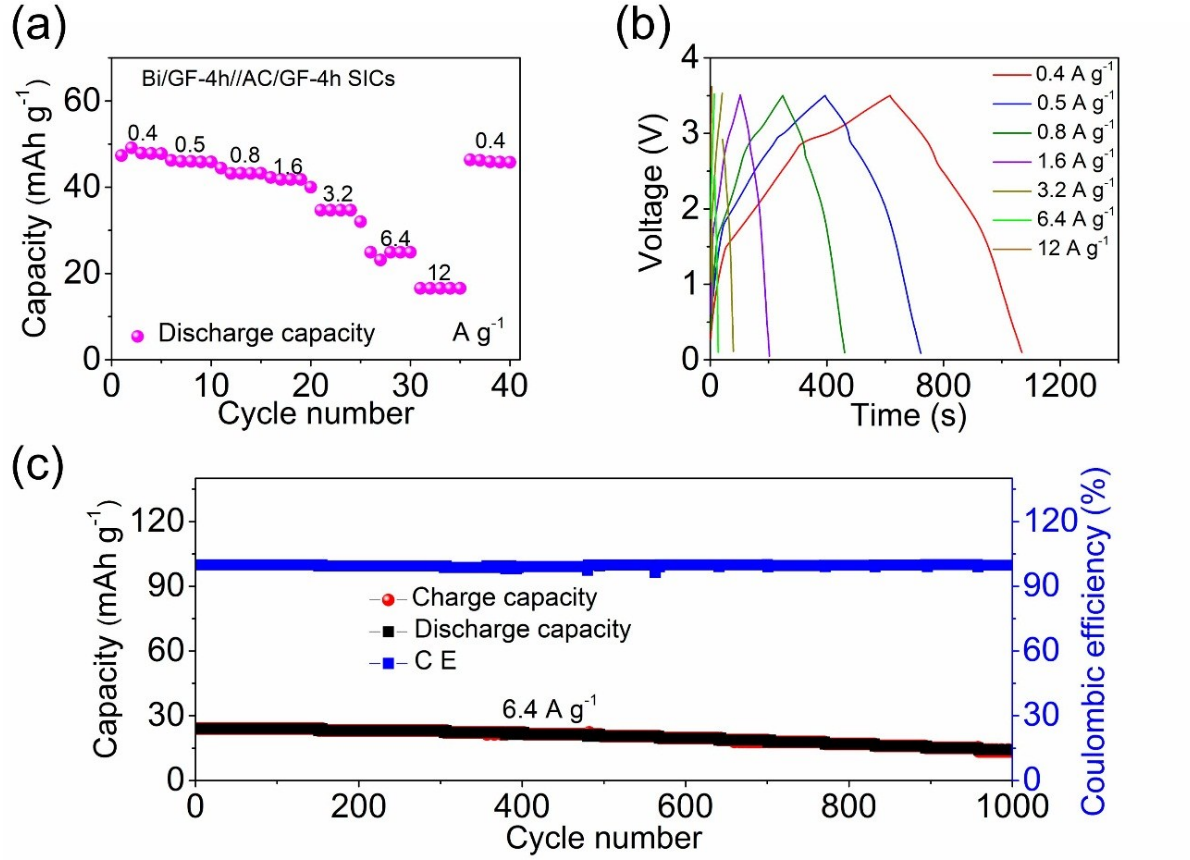

Fig. S27 Electrochemical performances of SICs based on Bi/GF-4h and AC/GF-4h fabrics electrodes: (a) Rate performance. (b) Galvanostatic charge/discharge curves at various current densities. (c) Cyclic life at the current density of 6.4 A g^{-1}.

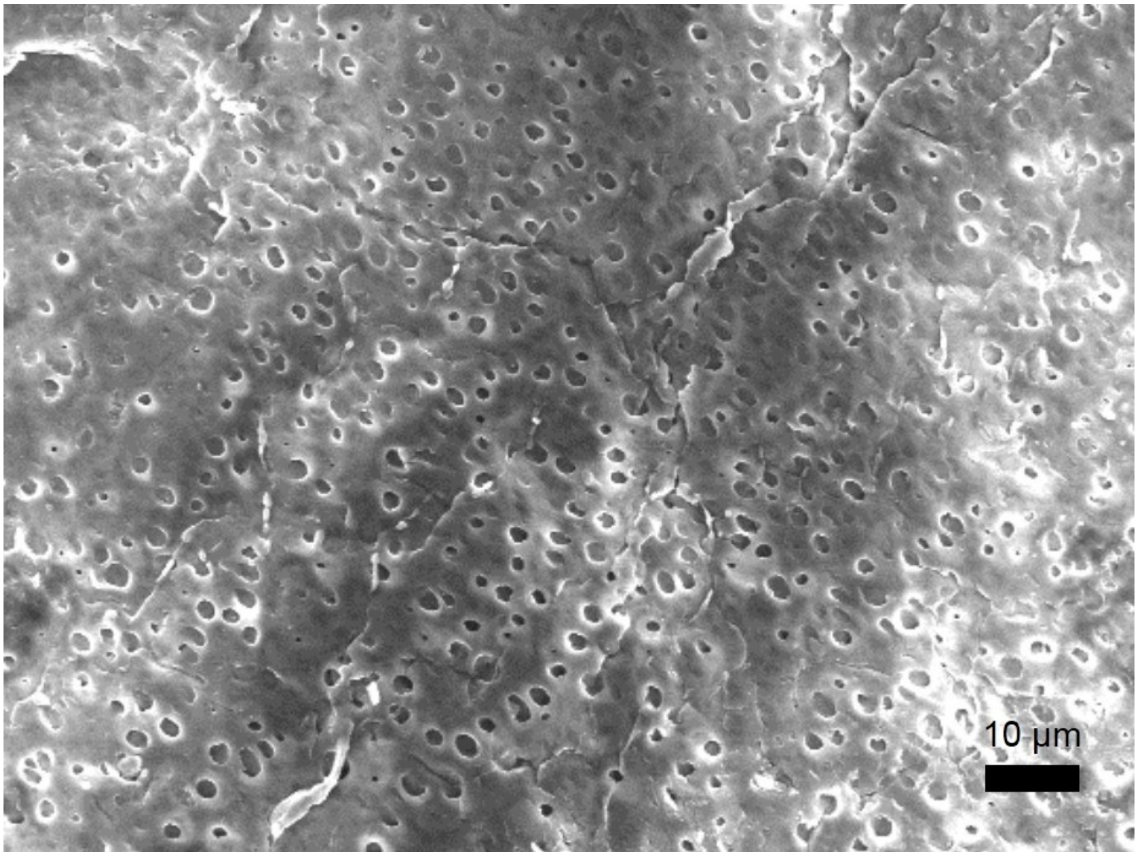

Fig. S28 SEM image of the pristine P(VDF-HFP) film.

Fig. S29 Thickness of the assembled device.

Reference

[1] Z. Liu, X. Zhang, D. Huang, B. Gao, C. Ni, L. Wang, Y. Ren, J. Wang, H. Gou, G. Wang, *Chem. Eng. J.* **2020**, 379, 122418.